Check for updates

DOI: 10.1002/zaac.202100342

Ca₂Ga₄Ge₆ and Ca₃Ga₄Ge₆: Synthesis, Structure, and Electronic Properties

Kelsey L. Hodge,^[a] H. Olivia Davis,^[a] Karl G. Koster,^[a] Wolfgang Windl,^[b] Curtis E. Moore,^[a] and Joshua E. Goldberger^{*[a]}

Dedicated to Mercouri Kanatzidis in celebration of his 65th birthday.

During the search for transition metal-free alkyne hydrogenation catalysts, two new ternary Ca–Ga–Ge phases, Ca₂Ga₄Ge₆ ($Cmc2_1$, a=4.1600(10) Å, b=23.283(5) Å, c=10.789(3) Å) and Ca₃Ga₄Ge₆ (C2/m, a=24.063(2) Å, b=4.1987(4) Å, c=10.9794(9) Å, β =91.409(4)°), were discovered. These compounds are isostructural to the previously established Yb₂Ga₄Ge₆ and Yb₃Ga₄Ge₆ analogues, and according to Zintl-Klemm counting rules, consist of anionic [Ga₄Ge₆]^{4–} and [Ga₄Ge₆]^{6–} frameworks in which every Ga and Ge atom would have a formal octet with no Ga–Ga or Ga–Ge π -bonding. These

compounds are metallic, based on temperature dependent electrical resistivity and thermopower measurements for $Ca_3Ga_4Ge_6$, along with density functional theory calculations for both phases. Unlike the highly active 13-layer trigonal CaGaGe phase, these new compounds exhibit minimal activity in the semi/full alkyne hydrogenation of phenylacetylene, which is consistent with previous observations that the lack of a formal octet for framework atoms is essential for catalysis in these Zintl-Klemm compounds.

Introduction

Intermetallic phases that combine electropositive group 1-3 elements with main group or late transition metal elements have a wealth of fascinating chemistry and many exotic physical properties. These properties include catalysis in BaGa2 and CaGaGe,^[1] topological phenomena and magnetism in EuSn₂As₂ and Euln₂P₂, [2] superconductivity in SrPtAs, [3] or structural phase transitions such as those observed in Sr_{1-x}Ca_xPdAs alloys. [4] Phases such as Yb₁₄MgSb₁₁ and Mg₃Bi₂, have been also extensively studied for applications in thermoelectrics. [5] The bonding of these phases is often dictated by Zintl-Klemm counting rules in which the electropositive elements donate electrons to the main group elements, which themselves form covalently bonded networks to achieve a full octet. Further work has emphasized how the structures of these phases can vary based on the changes in the cation and anion sizes, such as in A₂₁Cd₄Pn₁₈ (A=Eu, Sr, Ba; Pn=Sb, Bi). [6] Discovering new materials in this family has also led to new structural motifs such as the bell-like [Ga₅] polyanions in Sr₃Li₅Ga₅.^[7]

Recently, we discovered that transition metal-free layered Zintl-Klemm compounds with electronic structures that are

Lewis acidic such as BaGa2, YGa2, and a new 13-layer trigonal polytype of CaGaGe (13T-CaGaGe), exhibit extraordinary catalytic activities in the partial and full hydrogenation of phenylacetylene to styrene and ethylbenzene.^[1] These structures consist of honeycomb networks of main-group elements separated by the electropositive group 1-3 element/lanthanide. The Lewis acidity stems from the elements in the main group framework having either formally 7 valence electrons or weak intralayer π - π bonding. We hypothesized that the presence of 7 valence electrons would make these phases acidic, thereby promoting the adsorption of both H₂ and alkynes. By far, 13T-CaGaGe was the most catalytically active and oxidation-resistant catalyst, maintaining appreciable conversion after exposure to air for five months. Surprisingly, despite the presence of nine known binary Ca—Ga and five known binary Ca—Ge phases, [8] the only two reported ternary CaGaGe phases are 13T-CaGaGe and the 4-layer hexagonal CaGaGe polytype. In contrast, many other ternary (Ae/Ln)-Ga-Ge phases exist (Ae = divalent alkaline earth, Ln = divalent lanthanide Eu²⁺, Yb²⁺), such as Eu₄Ga₈Ge₁₆ and Sr₈Ga₁₆Ge₃₀ clathrate, [9] as well as Yb₂Ga₄Ge₆, and Yb₃Ga₄Ge₆ (Table 1).[10] Thus, we set out to explore whether other ternary Ca-Ga-Ge phases exist.

[a] K. L. Hodge, H. O. Davis, K. G. Koster, C. E. Moore, J. E. Goldberger Department of Chemistry and Biochemistry The Ohio State University 100 W. 18th Avenue, Columbus, OH 43210, United States E-mail: Goldberger.4@osu.edu

[b] W. Windl

Department of Materials Science and Engineering The Ohio State University 140 W. 19th Avenue, Columbus, OH 43210, United States

Supporting information for this article is available on the WWW under https://doi.org/10.1002/zaac.202100342

Table 1. Ternary phases including Ga and Ge with divalent alkaline earth (Ae) or lanthanide (Ln metals. *= this work here).					
Phase	Ca ²⁺	Sr^{2+}	Ba^{2+}	Eu^{2+}	Yb^{2+}
(Ae/Ln) ₄ Ga ₈ Ge ₁₆ (Ae/Ln) ₈ Ga ₁₆ Ge ₃₀ (Ae/Ln)GaGe	X ^[11]	X ^[9b] X ^[11]	X ^[9b] X ^[11]	X ^[9a] X ^[9b] X ^[12]	X ^[13] X ^[10]
(Ae/Ln)₂Ga₄Ge ₆ (Ae/Ln)₃Ga₄Ge ₆	*			X ^[10]	X ^[10]

Herein, we report two new phases in the Ca–Ga–Ge ternary system $Ca_2Ga_4Ge_6$ and $Ca_3Ga_4Ge_6$. These compounds are isostructural and isoelectronic analogs to the previously reported $Yb_2Ga_4Ge_6$ and $Eu_3Ga_4Ge_6$ structure types. In both structures, each Ga and Ge atom in the framework would formally feature 8 valence electrons considering electron donation from the Ca. These phases show negligible activity in the hydrogenation of phenylacetylene, in agreement with the expected lack of Lewis acidity. A combination of DFT calculations and electrical transport measurements show both compounds are metallic, similar to the Yb analogues.

Results and Discussion

Single crystals of $Ca_3Ga_4Ge_6$ were prepared by first arc melting together Ca:Ga:Ge in a 3:6:6 stoichiometry, followed by a crystal growth step in a Ga flux. The resulting $Ca_3Ga_4Ge_6$ product crystallized as needles with typical dimensions of 150–250 µm in diameter and 0.8–2 mm in length. From the single crystal diffraction data, a base-centered monoclinic Bravais lattice was established, and the analysis of the systematic extinctions led to 3 space groups (C2, Cm, and C2/m). Single crystal diffraction analysis confirmed that this phase was a C2/m space group. The fully solved single crystal structure of $Ca_3Ga_4Ge_6$ is shown in Figure 1, S1, Table 2, and Table 3. The solved crystal structure and the lattice constants closely resemble the previously established $Yb_3Ga_4Ge_6$ phase. The a, b, and c lattice constants of $Ca_3Ga_4Ge_6$ were within 0.06-0.12 Å of

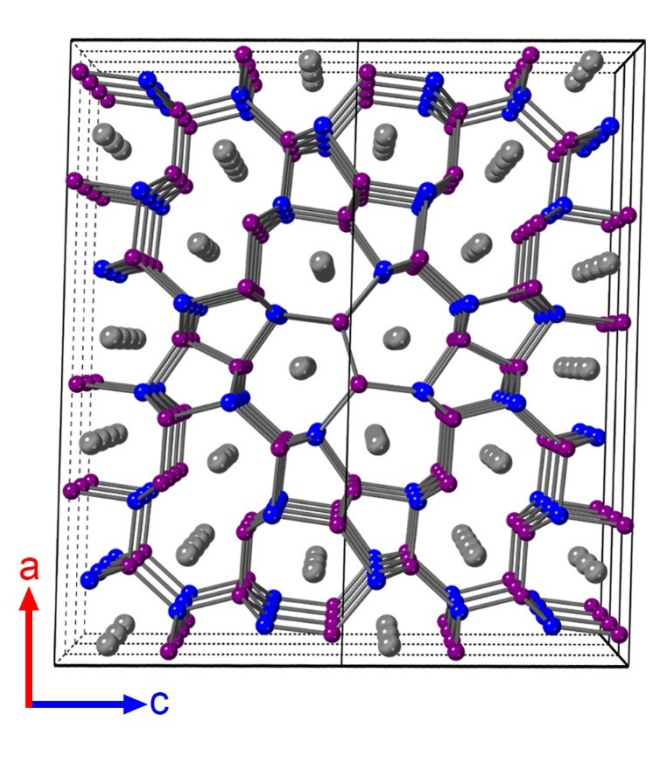


Figure 1. Crystal structure of $Ca_3Ga_4Ge_6$ looking down b axis with perspective view. Grey, blue, and purple spheres correspond to Ca, Ga, and Ge, atoms respectively.

Table 2. Crystal data and structure refinement for Ca ₃ Ga ₄ Ge _{6.}				
Empirical formula	Ca ₃ Ga ₄ Ge ₆			
Formula weight	834.66			
Temperature	298.15 K			
Wavelength	0.71073 Å			
Crystal system	Monoclinic			
Space group	C2/m			
a (Å)	24.063(2)			
<i>b</i> (Å)	4.1987(4)			
c (Å)	10.9794(9)			
β (°)	91.409(4)			
Volume (ų)	1108.96(17)			
Z	4			
Density (calculated) (Mg/m³)	4.999			
Absorption coefficient	26.89			
(mm ⁻¹)				
F(000)	1504			
Crystal size (mm)	$0.102 \times 0.044 \times 0.038$			
Crystal color, habit	Metallic Silver Block			
Theta range for data collec-	1.693 to 30.563°.			
tion				
Index ranges	$-32 \le h \le 34, -5 \le k \le 6,$			
	$-15 \le l \le 15$			
Reflections collected	16233			
Independent reflections	1883 [R(int) = 0.0388, R(sigma) -			
	=0.0223]			
Completeness to	100.00%			
theta $=$ 25.000 $^{\circ}$				
Absorption correction	Semi-empirical from equivalents			
Max. and min. transmission	0.0998 and 0.0456			
Refinement method	Full-matrix least-squares on F2			
Data/restraints/parameters	1883/0/80			
Goodness-of-fit on F2	1.089			
Final R indices [I > 2sigma(I)]	R1 = 0.0173, $wR2 = 0.0368$			
R indices (all data)	R1 = 0.0219, $wR2 = 0.0374$			
Extinction coefficient	0.00200(6)			
Largest diff. peak and hole (e	0.790 and -0.559			
$Å^{-3}$)				

Table 3. Atomic coordinates and equivalent isotropic displacement parameters (\mathring{A}^2) for $Ca_3Ga_4Ge_6$. U(eq) is defined as one third of the trace of the orthogonalized U^{ij} tensor.

	Х	у	Z	U(eq)
Ge(1)	0.39517(2)	0	0.63375(3)	0.0142(1)
Ge(2)	0.29161(2)	0	0.64436(3)	0.0128(1)
Ge(3)	0.44890(2)	1/2	0.96462(4)	0.0160(1)
Ge(4)	0.27456(2)	1/2	0.97437 (3)	0.0130(1)
Ge(5)	0.34770(2)	0	0.23628(3)	0.0123(1)
Ge(6)	0.47697(2)	1/2	0.39761(4)	0.0139(1)
Ga(1)	0.25891(2)	1/2	0.74453(4)	0.0135(1)
Ga(2)	0.36359(2)	1/2	0.11459(4)	0.0137(1)
Ga(3)	0.42065(2)	0	0.41322(3)	0.0111(1)
Ga(4)	0.56450(2)	1/2	0.27013(4)	0.0130(1)
Ca(1)	0.35541(3)	0	0.89321(7)	0.0149(2)
Ca(2)	0.47565(3)	0	0.16846(7)	0.0144(1)
Ca(3)	0.32264(3)	1/2	0.45448(7)	0.0175(2)

 $Yb_3Ga_4Ge_6$. Considering the Shannon ionic radii of Ca^{2+} and Yb^{2+} are within 0.02 Å of each other, it is unsurprising that these changes are subtle.^[10,14] Compared to the lattice parame-

ters of the Yb phase, Ca₃Ga₄Ge₆ is slightly smaller even though the Shannon ionic radius is larger.^[14] The size differences do, however, agree with the reported Eu₃Ga₄Ge₆.^[10] Additional data collected via single crystal XRD describing the bonding anisotropy are enumerated in Tables S1–2.

In this material, the Ca atoms can be thought of as donating electrons into the $[Ga_4Ge_6]^{6-}$ framework, consistent with the Zintl-Klemm concept. The local coordination of each of the Ca, Ga, and Ge atoms is depicted in Figure S2. The $Ca_3Ga_4Ge_6$ structure contains ten-, seven-, six- and five-membered rings (Figure 1). The ten-membered rings contain 2 Ca^{2+} ions between which spans a distance of 4.1987(12) Å. Ca(1) and Ca(2) reside within two different seven-membered ring tunnels.

The anionic $[Ga_4Ge_6]^{6-}$ framework contains four unique Ga sites which are exclusively coordinated by Ge in distorted tetrahedra and can be assigned a charge of -1, according to the Zintl-Klemm formalism. There are also six distinct Ge sites; four sites are four-coordinate distorted tetrahedra and two sites are three-coordinate. The electron donation by Ca partially reduces two of the 6 Ge atoms (Ge(3) and Ge(2)), breaking a Ge–Ge bond in the framework and leading to a Ge atom in trigonal pyramidal and trigonal planar geometry. There is not a charge assigned to the four-coordinate Ge atoms and the Ge sites that are three-coordinate are assigned a charge of -1. This results in an overall 6- charge on the $[Ga_4Ge_6]^{6-}$ framework, which is counterbalanced by 3 Ca^{2+} atoms.

Figure S2 displays the local coordination of each atomic site within the structure. Each of the Ga sites has a distorted tetrahedral geometry; Ga(1) has angles ranging from 92.421(17)–113.82(2)°. Ga(2) has 100.354(15)–117.17(12)° between its bond angles. Ga(3) has bond angles ranging from 102.182(14)–123.14(2)° and Ga(4) contains bond angles from 94.836(14)–117.43(2)°. The nearest neighbor Ga—Ge bond distances range from 2.5057(3)–2.6630(6) Å with an average of 2.548(45) Å.

The geometries of Ge are tetrahedral in the four-coordinate sites and either trigonal planar or trigonal pyramidal in the three-coordinate sites. The four Ge sites' bond angles are approximately tetrahedral with Ge(1) with 108.208(19)–111.99(2)°, Ge(4) with 99.520(19)–115.63(3)°, Ge(5) with 101.962(14)–126.640(19)°, and Ge(6) with 98.06(2)–119.422(12)°. Ge(2) is in a trigonal pyramidal environment with angles ranging from 110.179(14)–113.82(2)° with three Ga atoms forming the base. Ge(3) is in a distorted trigonal planar environment with bond angles between 113.39(2)–124.17(2)° which is relatively close to the 120° of a perfect trigonal planar molecule. Germanium is coordinated to both Ge and Ga and the average Ge—Ge bond distances are 2.500(31) Å.

The local coordination environments of the three Ca atoms of $Ca_3Ga_4Ge_6$ are shown in Figure S2. Within a radius of 3.6 Å, Ca (1) is surrounded by 13 atoms including both Ga and Ge atoms in its environment, while Ca (2) and Ca (3) are surrounded by only twelve. The range of Ca–Ge bond distances is from 2.9306(9)–3.4811(8) Å and the average Ca–Ge bond distance is 3.17(13) Å. As for Ca–Ga bonds, the range of distances is 3.0246(8)–3.5806(7) Å, with an average distance of

3.376 Å. The simulated and calculated diffraction patterns for $Ca_3Ga_4Ge_6$ are available in Figure S3.

Because of the similar X-ray scattering factors and anisotropic displacement parameters of Ga and Ge, it was difficult to conclusively determine the site occupancies of the Ga and Ge. To determine the Ga and Ge positions, we utilized a similar strategy to that which was reported for the initial determination of the structure of Yb₃Ga₄Ge₆. First, careful X-ray Fluorescence (XRF) analysis of the Ca₃Ga₄Ge₆ crystals was performed using a calibration curve, and indicated a Ga: Ge ratio of 3.94:6.0, confirming the stoichiometry of these neighboring elements (Figure 2). Second, since the covalent radius of Ge is slightly but still measurably smaller than that of Ga, we initially assigned the longer Ca-metal distances to Ca-Ga and the shorter ones to Ca-Ge. This resulted in an assignment of Ga and Ge positions as occurs in Yb₃Ga₄Ge₆. To confirm that this assignment was correct, Density Functional Theory (DFT) calculations were performed on four different structures in which certain Ga and Ge assignments were swapped. These alternate structures were chosen in an attempt to keep the longer Ca-metal distances to Ga, maximize the presence of Ga-Ge bonds, and minimize the presence of Ga-Ga bonds as the presence of homoatomic bonds of the minority component in four-bonded networks in clathrates are exceptionally rare. The original structure was found to be the most stable phase by -1 eV/unit cell (Table S3). Thus, these calculations strongly support the single crystal structure assignment. In addition, Ca has a Bader charge of 1.3, indicating an overall +2 oxidation state, and an anionic [Ga₄Ge₆]⁶⁻ framework.^[15] Future neutron diffraction studies could determine whether Ga and Ge site mixing occurs.

We also established a route to synthesize the orthorhombic phase Ca₂Ga₄Ge₆. Single crystals of this new ternary phase were also isolated from and found to be the majority product in a Ga flux reaction, in this case having a 1:15:3 stoichiometry of Ca: Ga: Ge. Minor impurity phases include Ca₃Ga₄Ge₆, and Ge.

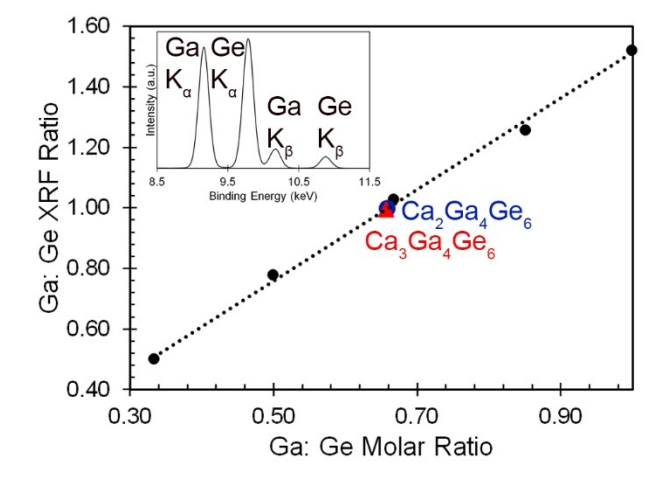


Figure 2. XRF calibration for the Ga: Ge ratio. The black circles correspond to the Ga_2O_3 :Ge mixtures used as standards and the blue circle and red triangle correspond to the $Ca_2Ga_4Ge_6$ and $Ca_3Ga_4Ge_6$, compounds tested respectively. The inset shows the XRF spectra of the Ga and Ge K_α and K_β peaks.

Figures 3, S4, Table 4, and Table 5 show the crystal structure that was elucidated from single crystal refinements, and it closely resembles the reported structure of Yb₂Ga₄Ge₆. It crystallizes into a polar orthorhombic space group *Cmc*2₁, and is constructed from a [Ga₄Ge₆]⁴⁻ framework. In this compound, each Ga site is 4-coordinate with a distorted tetrahedral coordination with neighboring Ge atoms (Figure S4). A myriad of tunnels are formed in this [Ga₄Ge₆]⁴⁻ framework, featuring Ga—Ge three-, five-, six-, seven-, and nine-membered rings. The Ca (1) and Ca (2) atoms reside within the holes of the seven-and nine-membered rings, respectively. Additional data collected via single crystal XRD fully detailing the bonding anisotropy are enumerated in Tables S4–S5.

Every Ga and Ge atom is covalently bonded to 4 other atoms in this framework, $[Ga_4Ge_6]^{4-}$, resulting in an octet for both atoms. In $Ca_2Ga_4Ge_6$, Ge is coordinated to both Ge and Ga, Ga is exclusively coordinated to Ge. The 2 Ca atoms donate a total of 4 electrons to the 4 different Ga atoms, thereby forming an octet.

There is a four-coordinate, nearly tetrahedral geometry for all Ga and Ge atoms (Figure S2). Ge(3) and Ge(4) have bond angles that are close to ideal tetrahedral geometries, ranging from 108.04(4)–113.70(6)° and 103.55(4)–114.94(6)°. Ge(2) and Ge(5) are more distorted with Ge(1) bond angles ranging from 91.23(5)–117.89(3)° and 101.06(4)–125.60(6)° for Ge(2). Ge(1) and (6) have very distorted geometries with angles ranging from 61.24(5)–123.83(3)° and 58.88(4)–124.54(3)°, respectively. The average Ge–Ge bond distance at 2.539(29) Å is very similar

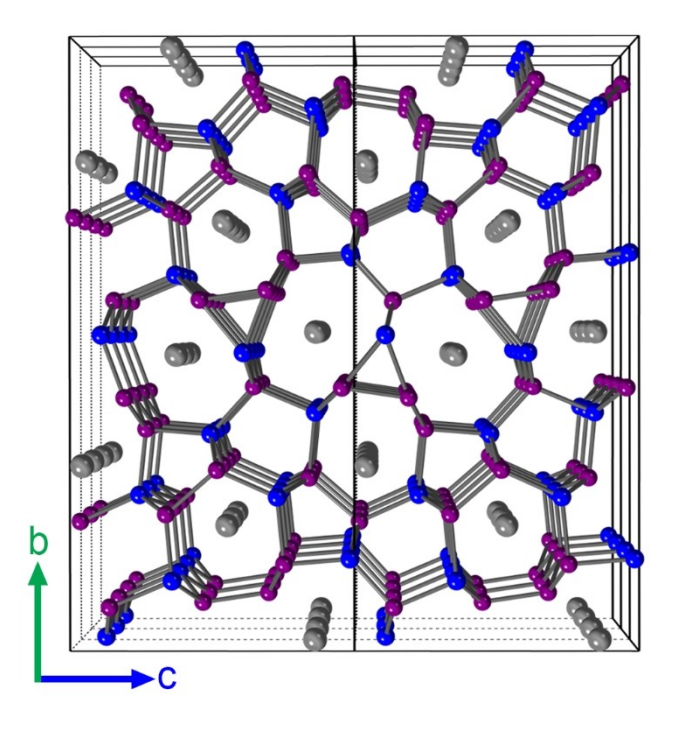


Figure 3. Crystal structure of $Ca_2Ga_4Ge_6$ with view down a axis. Grey, blue, and purple spheres correspond to Ca, Ga, and Ge, atoms respectively.

Table 4. Crystal data and struc	cture refinement for Ca ₂ Ga ₄ Ge ₆ .			
Empirical formula Ca ₂ Ga ₄ Ge ₆				
Formula weight	794.58			
Temperature	298.15 K			
Wavelength	0.71073 Å			
Crystal system	Orthorhombic			
Space group	Cmc2 ₁			
a (Å)	4.1600(10)			
b (Å)	23.283(5)			
c (Å)	10.789(3)			
Volume (ų)	1045.0(4)			
Z	4			
Density (calculated) (Mg/m³)	5.051			
Absorption coefficient (mm ⁻¹)	28.043			
F(000)	1424			
Crystal size (mm)	$0.327 \times 0.154 \times 0.069$			
Crystal color, habit	Metallic Silver Block			
Theta range for data collec-	1.749 to 30.544			
tion (°)				
Index ranges	$-5 \le h \le 5, -32 \le k \le 32,$			
	–15 ≤ l ≤ 15			
Reflections collected	17751			
Independent reflections	1784 [R(int) = 0.0559, R(sigma) - = 0.0322]			
Completeness to	99.80%			
theta = 25.000°				
Absorption correction	Semi-empirical from equivalents			
Max. and min. transmission	0.0511 and 0.0134			
Refinement method	Full-matrix least-squares on F ²			
Data/restraints/parameters	1784/1/74			
Goodness-of-fit on F2	1.04			
Final R indices [I > 2sigma(I)]	$R_1 = 0.0228$, $wR_2 = 0.0469$			
R indices (all data)	$R_1 = 0.0266$, $wR_2 = 0.0477$			
Absolute structure parame-	0.01(2)			
ter				
Extinction coefficient	0.00120(14)			
Largest diff. peak and hole (e \mathring{A}^{-3})	0.658 and -0.791			

to that in elemental Ge, which has Ge–Ge bond lengths of 2.449 $\text{\AA}^{\text{[16]}}$

The Ga atoms are also generally in a distorted tetrahedral coordination geometry where the 4 nearest neighbors are Ge atoms. Ga(1) has bond angles ranging from 106.89(4)–127.24(6)°, Ga(3) from 101.83(4)–119.96(5)° and Ga(4) from 103.44(4)–115.33(3)°. By far the most distorted Ga atom is Ga(2) which contains a nearly equilateral triangular bonding arrangement with Ge(1) and Ge(6), with bond lengths ranging from 2.5370(16)–2.5981(17) Å and bond angles ranging from 58.88(4)–61.24(5)°. The analogous Yb₂Ga₄Ge₆ structure shares this same unique, three-membered, triangular Ge₂Ga rings, which are occasionally observed in other compounds featuring group 13 atoms. Previous reports of similar three membered rings include Sr₂Au₆Ga₃ and Eu₂Au₆Ga₃, both of which contain Ga₃ triangular units. [17]

While the triangular moiety is rare, the overall Ga–Ge interactions are strong and have an average bond distance of 2.51(4) Å which agrees with the 2.51 Å Ga–Ga bond distance reported by Kanatzidis *et. al* in $Yb_2Ga_4Ge_6$. Summing the

nloaded from https://onlinelibrary.wiley.com/doi/10.1002/zaac.202100342 by Ohio State University Ohio Sta, Wiley Online Library on [19/01/2025]. See the Terms and Conditions (https://onlinelibrary.wiley.com/erms

conditions) on Wiley Online Library for rules of use; OA articles are governed by the applicable Creative Commons

Table 5. Atomic coordinates and equivalent isotropic displacement paraments (\mathring{A}^2) for $Ca_2Ga_4Ge_6$. U(eq) is defined as one third of the orthogonalized U^{ij} tensor.

	X	у	Z	U(eq)
Ge(1)	0	0.58772(4)	0.80840(11)	0.0198(2)
Ge(2)	1/2	0.64135(5)	0.74738(9)	0.0206(2)
Ge(3)	1/2	0.57126(5)	0.36135(9)	0.0199(2)
Ge(4)	0	0.70536(5)	0.48322(9)	0.0196(2)
Ge(5)	1/2	0.72253(4)	0.16298(10)	0.0200(2)
Ge(6)	0	0.57158(5)	0.04346(9)	0.0192(2)
Ga(1)	1/2	0.64991(5)	0.51578(9)	0.0190(2)
Ga(2)	0	0.51446(5)	0.39011(10)	0.0220(2)
Ga(3)	0	0.74945(5)	0.27127(9)	0.0191(2)
Ga(4)	1/2	0.61417(4)	0.14138(10)	0.0204(2)
Ca(1)	0	0.69859(9)	0.9570(2)	0.0231(4)
Ca(2)	1/2	0.51897(9)	0.6387(2)	0.0222(4)

average radius of Ga from its crystal structure (1.33 Å) and the covalent radius of Ge (1.22 Å) yields a distance of 2.55 Å, indicating strong covalent bonding between Ga and Ge in the rigid $[Ga_aGe_a]^{4-}$ network.

The coordination environments of the two unique Ca atoms are shown in Figure S5. Ca(1) has 14 atoms in its coordination sphere, 8 are germanium and 6 are gallium. The Ca-Ge distances range from 3.039(2)-3.666(3) Å with an average distance in the coordination sphere of 3.28(23) Å. Ca(2) has a coordination number of 13 consisting of 7 germanium and 5 gallium atoms. The Ca-Ga distances fall between 3.081(2)-3.5059(19) Å with the average distance in the coordination sphere of 3.26(15) Å. The lattice constants and bond distances are also similar to that of Yb2Ga4Ge6. [10] Again, the Shannon crystal radius of Ca²⁺ is only 0.02 Å larger than Yb²⁺ for the 6, 7, and 8 coordination numbers that are enumerated. [14] XRF analysis of the isolated Ca2Ga4Ge6 crystals indicated a Ga:Ge ratio of ~3.96:6, again confirming the stoichiometry of these neighboring elements (Figure 2). To elucidate the Ga and Ge positions in the unit cell, we utilized a similar strategy that was described above for Ca₃Ga₄Ge₆. DFT energies of four different structures in which specific Ga and Ge assignments were swapped indicated that this structure was the most stable phase by -1 eV/unit cell (Table S6). These DFT calculations strongly support the assignment of Ga and Ge at specific Wyckoff positions in the single crystal structure determination. Finally, Ca is again calculated to have a Bader charge of 1.3, which indicates an overall +2 oxidation state and an anionic [Ga₄Ge₆]⁴⁻ framework.^[15]

DFT calculations were also carried out to determine the electronic structure of both $\text{Ca}_2\text{Ga}_4\text{Ge}_6$ and $\text{Ca}_3\text{Ga}_4\text{Ge}_6$ (Figure 4). The band structures of $\text{Ca}_2\text{Ga}_4\text{Ge}_6$ and $\text{Ca}_3\text{Ga}_4\text{Ge}_6$ are available in Figure 4 a, c. Both materials are metallic with multiple bands crossing the Fermi level (E_F). Figure 4 b, d also shows the atomresolved density of states (DOS) plots of these two materials at energies close to E_F. In both materials, E_F lies in a pseudogap. Additionally, at E_F in both compounds, the density of states increases with lower energies, which would suggest holes as the dominant carrier type. [18]

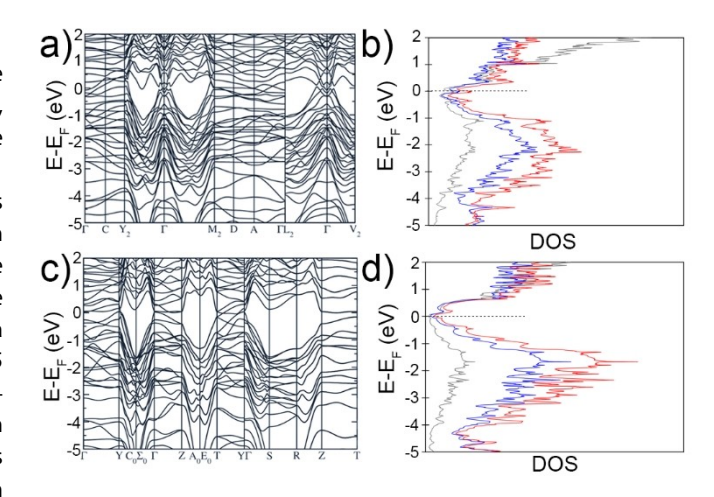


Figure 4. Band structure diagrams for a) Ca₃Ga₄Ge₆ and c) Ca₂Ga₄Ge₆. Atom-resolved DOS plots for b) Ca₃Ga₄Ge₆ and d) Ca₂Ga₄Ge₆, respectively. Gray, blue and red lines represent the partial DOS from calcium, gallium, and germanium, respectively.

Measurements of the electronic properties of sintered pellets of Ca₃Ga₄Ge₆ also indicate metallic behavior. Exceptional care was taken to ensure that no residual Ga flux was incorporated into the sintered pellet, as this would provide an electrical short that would convolute the transport data. The presence of residual Ga flux was noticeable in the powder XRD (Figure S6) and would lead to a metallic coating on an agate mortar and pestle upon grinding. To remove this trace Ga flux, we ground the powder in a warm mortar and pestle, cleaned away the Ga coating with HCl, and repeated this procedure multiple times until no further Ga coating was apparent on the mortar and pestle, and no Ga peaks were apparent in the powder XRD spectrum. Unfortunately, growing and separating a sufficiently large quantity of pure material of Ca₂Ga₄Ge₆ for electronic transport measurements proved challenging. The powder X-ray diffraction of the majority Ca₂Ga₄Ge₆ phase separated from the flux indicated the presence of residual Ca₃Ga₄Ge₆, Ge, and Ga impurities (Figure S7).

Figure 5 shows the electrical resistivity, thermopower, and thermal conductivity of Ca₃Ga₄Ge₆. The room temperature

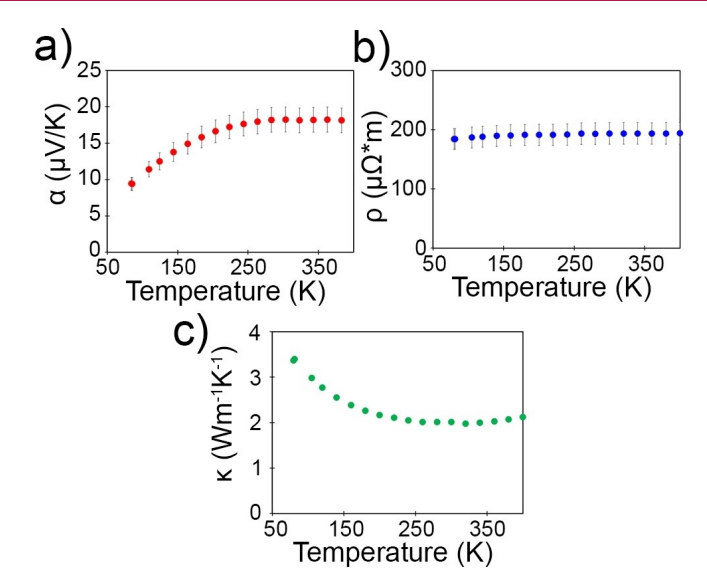


Figure 5. a) Seebeck, b) resistivity and c) thermal conductivity of $Ca_3Ga_4Ge_6$.

resistivity of this sintered Ca₃Ga₄Ge₆ pellet is relatively low (~ 190 $\mu\Omega$ m) and decreases with decreasing temperature. The relatively low resistivity and the temperature trend are indicative of metallic behavior (Figure 5a), albeit a poor metal. The room temperature resistivity of Ca₃Ga₄Ge₆ is two orders of magnitude higher than previous measurements on single crystals of Yb₃Ga₄Ge₆ (1.4 $\mu\Omega$ m). The much larger resistivity of this sintered Ca₃Ga₄Ge₆ pellet is likely a consequence of the multitude of grain boundaries. Althugh extraordinary care was taken to completely remove any detectable traces of Ga via Xray diffraction, it is possible that the observed metallic behavor was due to the presence of metallic material such as Ga coating the grains. Still, the observed metallic conductivity is strongly supported by band structure calculations. The thermopower ranges from 9–18 μ V K⁻¹ from 80–400 K (Figure 5a). The small value is consistent with the metallic nature of the compound and the positive values confirm holes to be the dominant carrier type. The thermal conductivity of the sintered pellet is also guite small and ranges from 3.5 to 2 W m⁻¹ K⁻¹ (Figure 5b). The thermal conductivity is dominated by the lattice component as the electronic portion of the thermal conductivity estimated using the Wiedemann-Franz law (assuming a Lorenz number of $2.44 \times 10^{-8} \text{ W}\Omega \text{ K}^{-2}$) is only $\sim 0.04 \text{ W} \text{ m}^{-1} \text{ K}^{-1}$ at 300 K (Figure 5c). The low lattice thermal conductivity value is expected due to the multitude of grain boundaries in the sintered pellet, along with the relatively large and complex unit cell of the material.

Finally, considering the similar atomic composition to the highly active alkyne hydrogenation catalyst 13T-CaGaGe, [1a,b] $Ca_2Ga_4Ga_6$ and $Ca_3Ga_4Ge_6$ were explored for their ability to hydrogenate phenylacetylene to styrene and/or ethylbenzene. Under 51 bar H_2 , 8 mol% catalyst, 90 °C, and 24 h, 0.91 mmol phenylacetylene, in 2.4 mL n-butanol solvent, 13T-CaGaGe completely converts phenylacetylene to styrene and ethyl-

benzene. Using these same conditions $Ca_2Ga_4Ge_6$, $Ca_3Ga_4Ge_6$, and a control experiment with no catalyst typically led to <7% conversion. Thus, $Ca_2Ga_4Ge_6$ and $Ca_3Ga_4Ge_6$ show negligible activity. As the Ga and Ge atoms in these frameworks have formal octets according to the Zintl-Klemm formalism, the lack of catalytic activity with these compounds is due to the absence of Lewis acidity on the framework. [1a]

Conclusions

Two new compounds, Ca₃Ga₄Ge₆ and Ca₂Ga₄Ge₆, have been synthesized as single crystals from gallium flux. These compounds are built from [Ga₄Ge₆]ⁿ⁻ frameworks that are counterbalanced with Ca²⁺ ions. Calculations and measurements indicate that both are metallic. Consistent with our previously established design principles for Zintl-Klemm phase catalysts, these materials are not catalytically active. Considering the complexity of the binary Ca–Ga and Ca–Ge phase diagrams as well as other ternary phases containing Ga and Ge, it is likely that many more ternary Ca–Ga–Ge phases exist that feature exotic properties.

Experimental Section

Synthesis of Ca $_2$ **Ga** $_4$ **Ge** $_6$ **and Ca** $_3$ **Ga** $_4$ **Ge** $_6$: Single crystals of both Ca} $_2$ Ga $_4$ Ge $_6$ and Ca}_3Ga $_4$ Ge $_6$ were synthesized using a gallium flux method. Ca}_2Ga $_4$ Ge $_6$ crystals were prepared by weighing out amounts of Ca granules (Strem, 99.5% purity), Ga (Acros, 99.99%) and Ge (Alfa, Aesar, 99.999% purity) in 1:15:3 ratio (Ca 2.52 mmol, Ga 37.7 mmol, Ge 7.55 mmol) The mixture was heated to 800°C over 10 hours, held at 800°C for 36 hours, and cooled to 200°C over 18 hours. The resultant flux was centrifuged to reveal single crystals, with an overall yield of 94%.

 ${\rm Ca_3Ga_4Ge_6}$ crystals were prepared by weighing out amounts of Ca, Ga, and Ge in 1:2:2 ratio (Ca 2.48 mmol, Ga 4.93 mmol, Ge 4.92 mmol) and arc melted under positive pressure of argon via a thoriated tungsten electrode. The resulting button was ground in a Diamonite mortar and pestle (mass of powder 0.4518 g) and transferred into a quartz ampule. Excess gallium (19.6 mmol) was added as flux. The tube was evacuated and sealed. It was then placed in a vertical furnace. It was heated to 800 °C over 4 hours, held for 24 hours, and then cooled to 25 °C over 4 hours. The resulting ingot was warmed with a heat gun to melt the gallium and transferred into a centrifuge tube with quartz wool and centrifuged for 90 seconds at 3000 rpm. Yield was 99 %.

Powder X-ray diffraction: PXRD patterns were collected from the flux-grown crystals that were ground into a powder and collected using Johansson geometry. A Bruker D8 Advance Powder XRD with a monochromated Cu $K_{\alpha 1}$ source was used at a wavelength of 1.5406 Å.

Microscope Images: Images were collected by Olympus EX41 Optical microscope equipped with OptixCam Summit Series for capturing images.

X-ray Fluorescence: X-ray fluorescence was used to elucidate the Ga: Ge ratio of the final compounds. A calibration curve was prepared by weighing out Ge and Ga₂O₃ powders with Ga: Ge molar ratios ranging from 2:6–6:6. Data was collected via Thermo

Scientific ARL QUANT'X EDXRF Analyzer using a palladium medium filter (Mid Zb).

DFT calculations: For the DFT calculations, we used the VASP code^[19] with PAW PBE potential,^[20] a Γ -centered k-point mesh for Brillouin zone integration with a k-spacing of 0.1 Å $^{-1}$, and a kinetic-energy cutoff for plane-wave expansion of 217 eV. For the band structure, the experimental lattice constants were held fixed, while the atomic positions were allowed to relax. The primitive files and k-space paths for band structure calculations were generated with the SeeK-path online tool.^[21] For determining the Ga and Ge assignment, the energy of the different structures was calculated by fixing the experimental lattice constants and relaxing the atomic positions, as well as relaxing both the lattice constants and atomic positions which yielded very similar results.

Single crystal refinements: Ca₂Ga₄Ge₆: The single crystal X-ray diffraction studies were carried out on a Nonius Kappa diffractometer equipped with a Bruker APEX-II CCD and Mo K_{α} radiation (λ = 0.71073 Å). A $0.327 \times 0.154 \times 0.069$ mm³ piece of a metallic silver block was mounted on a Cryoloop with clear enamel. Data were collected at ambient condition using ϕ and ϖ scans. Crystal-todetector distance was 40 mm and exposure time was 10 seconds per frame using a scan width of 1.0°. Data collection was 99.8% complete to 25.00° in θ . A total of 17751 reflections were collected covering the indices, $-5 \le h \le 5$, $-32 \le k \le 32$, $-15 \le l \le 15$. 1784 reflections were found to be symmetry independent, with an R_{int} of 0.0559. Indexing and unit cell refinement indicated a C-centered. orthorhombic lattice. The space group was found to be Cmc2₁. The data were integrated using the Bruker SAINT software program and scaled using the SADABS software program. Solution by direct methods (SHELXT) produced a complete model for the phase problem for refinement. [22] All atoms were refined anisotropically by full-matrix least-squares (SHELXL-2014).[23] The absolute stereochemistry of the material was established by anomalous dispersion using the Parson's method with a Flack parameter of 0.006(22).

Ca₃Ga₄Ge₆: The single crystal X-ray diffraction studies were carried out on a Nonius Kappa diffractometer equipped with a Bruker APEX-II CCD and Mo K_a radiation (λ =0.71073 Å). A 0.102×0.044× 0.038 mm³ piece of a metallic silver block was mounted on a Cryoloop with clear enamel. Data were collected at ambient condition using ϕ and ϖ scans. Crystal-to-detector distance was 40 mm and exposure time was 10 seconds per frame using a scan width of 1.0°. Data collection was 100% complete to 25.00° in θ . A total of 16233 reflections were collected covering the indices, -32 < h < 34, -5 < k < 6, -15 < l < 15. 1883 reflections were found to be symmetry independent, with an R_{int} of 0.0388. Indexing and unit cell refinement indicated a C-centered, monoclinic lattice. The space group was found to be C2/m. The data were integrated using the Bruker SAINT software program and scaled using the SADABS software program. Solution by direct methods (SHELXT) produced a complete model for the phase problem for refinement. All atoms were refined anisotropically by full-matrix least-squares (SHELXL-2014).

Electronic and thermal transport measurements: The Seebeck coefficients, resistivities, and thermal conductivities of sintered $\text{Ca}_3\text{Ga}_4\text{Ge}_6$ pellets were measured from 80 K to 400 K in a Janis liquid nitrogen vacuum cryostat. A four-probe measurement geometry was used to measure sample resistance. For thermal conductivity and thermopower measurements, current was passed through a 120 Ω Omega strain gauge to apply heat to one end of the sample while two type T thermocouples measured the resulting temperature gradient and Seebeck voltage. The thermocouples, resistive heater, and current wires were attached to the sample using Epo-Tek H2OE silver epoxy cured at 135 °C.

The errors of thermopower and resistivities were propagated based on the value of $\Delta L_T/L_T$, or the diameter of silver epoxy used to affix copper (voltage) wires to the sample divided by the length between the wires. Care was taken to use as little silver epoxy paste as possible to minimize heat dissipation from the sample through the electrical contacts. Sample cross-sectional areas were measured both manually with calipers and digitally with image processing software to confirm the dimensions.

Acknowledgements

This work was primarily supported by the Center for Emergent Materials an NSF MRSEC, under Award DMR-2011876. W.W.'s contributions were funded by the AFOSR, Award FA9550-21-1-0268, program director Dr. Ali Sayir. W.W. thanks the Ohio Supercomputer Center for supercomputing resources under project number PA0072.

Conflict of Interest

The authors declare no conflict of interest.

Data Availability Statement

The data that support the findings of this study are available from the corresponding author upon reasonable request.

Keywords: Intermetallics · Zintl Phases · Solid-state materials

- a) K. L. Hodge, J. E. Goldberger, ACS Appl. Mater. Interfaces 2021, 13, 52152–52159; b) K. L. Hodge, M. B. Gray, W. Windl, J. E. Goldberger, Inorg. Chem. 2021, 60, 14530–14534; c) K. L. Hodge, J. E. Goldberger, J. Am. Chem. Soc. 2019, 141, 19969– 19972.
- [2] a) M. Q. Arguilla, N. D. Cultrara, Z. J. Baum, S. Jiang, R. D. Ross, J. E. Goldberger, *Inorg. Chem. Front.* **2017**, *4*, 378–386; b) J. Jiang, S. M. Kauzlarich. *Chem. Mater.* **2006**, *18*, 435–441.
- [3] Y. Nishikubo, K. Kudo, M. Nohara, J. Phys. Soc. Jpn. 2011, 80, 055002.
- [4] B. W. Y. Redemann, M. R. Scudder, D. Weber, Y. X. Wang, W. Windl, J. E. Goldberger, *Inorg. Chem. Front.* 2020, 7, 2833–2839.
- [5] a) J. Mao, H. Zhu, Z. Ding, Z. Liu, G. A. Gamage, G. Chen, Z. Ren, Science 2019, 365, 495–498; b) Y. Hu, J. Wang, A. Kawamura, K. Kovnir, S. M. Kauzlarich, Chem. Mater. 2015, 27, 343–351.
- [6] S.-Q. Xia, S. Bobev, Inorg. Chem. 2008, 47, 1919-1921.
- [7] M. Kotsch, Y. Prots, A. Ormeci, A. Senyshyn, M. Kohout, Y. Grin, Z. Anorg. Allg. Chem. 2021, 647, 1797–1803.
- [8] a) A. Palenzona, P. Manfrinetti, M. L. Fornasini, J. Alloys Compd. 2002, 345, 144–147; b) H. Okamoto, in Binary Alloy Phase Diagrams, Vol. 1, II ed., 1990, pp. 913–914.
- [9] a) J. D. Bryan, G. D. Stucky, Chem. Mater. 2001, 13, 253–257;
 b) B. C. Sales, B. C. Chakoumakos, R. Jin, J. R. Thompson, D. Mandrus, Phys. Rev. B: Condens. Matter Mater. Phys. 2001, 63, 245113.
- [10] M. A. Zhuravleva, J. Salvador, D. Bilc, S. D. Mahanti, J. Ireland, C. R. Kannewurf, M. G. Kanatzidis, Chem. Eur. J. 2004, 10, 3197– 3208.

RESEARCH ARTICLE

Downloaded from https://onlinelibrary.wiley.com/doi/10.1002/zaac.202100342 by Ohio State University Ohio Sta, Wiley Online Library on [19/01/2025]. See the Terms

of use; OA

articles are governed by the applicable Creative Commons

- [11] a) M. J. Evans, Y. Wu, V. F. Kranak, N. Newman, A. Reller, F. J. Garcia-Garcia, U. Haussermann, Phys. Rev. B: Condens. Matter Mater. Phys. 2009, 80, 064514; b) A. Czybulka, B. Pinger, H.-U. Schuster, Z. Anorg. Allq. Chem. 1989, 579, 151–157.
- [12] T.-S. You, Y. Grin, G. J. Miller, Inorg. Chem. 2007, 46, 8801–8811.
- [13] Y. Janssen, S. Chang, B. K. Cho, A. Llobet, K. W. Dennis, R. W. McCallum, R. J. McQueeney, P. C. Canfield, J. Alloys Compd. 2005, 389, 10–13.
- [14] R. D. Shannon, Acta Crystallogr. Sect. A 1976, 32, 751–767.
- [15] S. Posysaev, O. Miroshnichenko, M. Alatalo, D. Le, T. S. Rahman, *Comput. Mater. Sci.* **2019**, *161*, 403–414.
- [16] A. S. Cooper, Acta Crystallogr. 1962, 15, 578-582.
- [17] B. Gerke, A. Korthaus, O. Niehaus, F. Haarmann, R. Pottgen, Z. Naturforsch. B 2016, 71, 567–577.
- [18] Y. X. Wang, K. G. Koster, A. M. Ochs, M. R. Scudder, J. P. Heremans, W. Windl, J. E. Goldberger, J. Am. Chem. Soc. 2020, 142, 2812–2822.
- [19] a) G. Kresse, J. Furthmuller, Phys. Rev. B: Condens. Matter Mater. Phys. 1996, 54, 11169–11186; b) G. Kresse, J. Furthmuller,

- Comput. Mater. Sci. **1996**, 6, 15–50; c) G. Kresse, J. Hafner, *Phys. Rev. B: Condens. Matter Mater. Phys.* **1994**, 49, 14251–14269.
- [20] a) P. E. Blochl, Phys. Rev. B: Condens. Matter Mater. Phys. 1994, 50, 17953–17979; b) G. Kresse, D. Joubert, Phys. Rev. B 1999, 59, 1758–1775.
- [21] a) Y. Hinuma, G. Pizzi, Y. Kumagai, F. Oba, I. Tanaka, Comput. Mater. Sci. 2017, 128, 140–184; b) A. Togo, I. Tanaka, arXiv:1808.01590, 2018.
- [22] a) G. M. Sheldrick, Acta Crystallogr. Sect. A 2007, 64 112–122;
 b) G. M. Sheldrick, Acta Crystallogr. Sect. A 2015 71, 3–8.
- [23] G. M. Sheldrick, Acta Crystallogr. Sect. C 2015, 71, 3-8.

Manuscript received: November 12, 2021 Revised manuscript received: January 21, 2022 Accepted manuscript online: January 28, 2022